The University of Tehran Press

Pollution

https://jpoll.ut.ac.ir/

Print ISSN: 2383-451X
Online ISSN: 2383-4501

Low-Temperature Fabrication of a CuO/CNT Nanocomposite Derived from CNTs Grown on Activated Carbon for Visible-Light-Driven Dye Degradation

Wafa Sarhan Al Saidi[1,2], Saima Farooq[1], Salam Kadhim Al Dawery[3], Mohammed Al-Saadi[3], Dunaboyina Sri Maha Vishnu[1,2], Badar Al Nairi[2], Issa Sulaiman Al Amri[1], Ahmed Suliaiman Fadhil Al Harrasi[2], Sreedhar Reddy Sajjala[4]✉

1. Department of Biological Sciences and Chemistry, University of Nizwa, Nizwa-616, Oman
2. Natural and Medicinal Sciences Research Center, University of Nizwa, Nizwa-616, Oman
3. Chemical and Petrochemical Engineering, College of Engineering and Architecture, University of Nizwa, Nizwa-616, Oman
4. Department of Civil and environmental Engineering, College of Engineering and Architecture, University of Nizwa, Nizwa-616, Oman

Article Info

Article type:
Research Article

Article history:
Received: 20 Apr 2026
Revised: 16 Jul 2026
Accepted: 12 Sep 2026

Keywords:
CuO/CNT Nanocomposite
Photocatalytic degradation
Wastewater Treatment
SDG
Advanced Oxidation Processes

ABSTRACT

This study presents a facile synthesis of a CuO/CNT nanocomposite using pristine CNTs grown on powdered activated carbon at a low temperature of 250 °C, demonstrating efficient visible-light dye degradation under 6 W LED irradiation. Detailed material characterization confirmed the formation of well-dispersed CuO nanoparticles (7–12 nm) clustered around CNTs and exhibiting a tube-like morphology (50–120 nm), which enhanced structural stability and catalytic performance. The CuO/CNT nanocomposite exhibited high photocatalytic efficiency, achieving 90% degradation of Methyl Green (MG) and 67% degradation of Methyl Orange (MO) within 180 minutes under visible-light irradiation. Kinetic studies revealed that the dye degradation followed a pseudo-first-order model, with rate constants of 0.0081 min^{-1} for MG and 0.005 min^{-1} for MO. The incorporation of CNTs enhanced charge separation, light absorption, and reaction kinetics, thereby overcoming the limitations of pure CuO. These findings indicate that CuO/CNT is an efficient and economical photocatalyst for degrading organic pollutants in wastewater treatment applications, contributing to the achievement of several Sustainable Development Goals (SDGs).

Cite this article: Al Saidi, W. S., Farooq, S., Al Dawery, S. K., Al-Saadi, M., Vishnu, D. S. M., Al Nairi, B., Al Amri, I. S., Al Harrasi, A., & Reddy, S. (2026). Low-Temperature Fabrication of a CuO/CNT Nanocomposite Derived from CNTs Grown on Activated Carbon for Visible-Light-Driven Dye Degradation. *Pollution*, 12(3), 953-970. https://doi.org/10.22059/poll.2026.413052.3313

 Publisher: The University of Tehran Press.
DOI: https://doi.org/10.22059/poll.2026.413052.3313

INTRODUCTION

Dyes are synthetic organic compounds widely used in the textile and dyeing industries (Demarema *et al.*, 2024; Rahmati *et al.*, 2021; Mohammed *et al.,* 2018). Approximately 15% of commercially used dyes are discharged into the environment through untreated wastewater effluents, posing a major source of water pollution due to their toxicity and non-biodegradable nature (Kumar *et al.,* 2025; Shaban and Ashraf, 2018; Mahmoodi *et al.,* 2016). Their high chemical stability makes them resistant to conventional treatment methods such as biodegradation, adsorption, coagulation–flocculation, and chemical oxidation, allowing them to persist in the environment for extended periods (Mahmoodi *et al.,* 2016). Consequently,

*Corresponding Author Email: *sreedharreddy@unizwa.edu.om*

advanced oxidation processes (AOPs) have gained considerable attention for degrading recalcitrant pollutants through the generation of highly reactive hydroxyl radicals (Kumar *et al.,* 2025; Mahmoodi *et al.,* 2016; Singh *et al.,* 2025).

Among various AOPs, heterogeneous photocatalytic degradation has emerged as a promising technique for the mineralization of refractory organic pollutants under natural or simulated visible light (Lau *et al.,* 2020; Rochkind *et al.,* 2014; Al-Qaradawi and Salman, 2002; Nguyen *et al.,* 2019; Sapkota *et al.,* 2020). Its low operational cost, simplicity, and ability to generate strong oxidizing radicals under solar irradiation make it advantageous over many conventional treatment technologies (Rahmati *et al.,* 2021; Shaban and Ashraf, 2018; Mahmoodi *et al.,* 2016; Sapkota *et al.,* 2020; Salama *et al.,* 2018; Kumar, 2017; Kumar and Pandey, 2017).

Transition metal oxide nanoparticles have been extensively investigated for photocatalytic applications (Mohammed *et al.,* 2018; Mahmoodi *et al.,* 2016). Among them, copper(II) oxide (CuO), a p-type semiconductor with a narrow band gap (1.2–2.6 eV), has attracted significant attention because of its low cost, chemical stability, low toxicity, catalytic activity, and facile synthesis (Sapkota *et al.,* 2020; Moumen *et al.,* 2022). CuO has been employed in various applications, including energy storage, photovoltaics, gas sensors, and photocatalysis (Sapkota *et al*., 2020; Baqer *et al*., 2018). However, its photocatalytic efficiency is limited by rapid electron–hole recombination and relatively weak visible-light absorption (Mahmoodi *et al.,* 2016; Sapkota *et al.,* 2020). Therefore, introducing suitable co-catalysts or dopants is necessary to enhance its photocatalytic performance.

Carbon nanotubes (CNTs) are among the most promising carbon-based support materials because of their large surface area, excellent thermal and electrical conductivity, high chemical stability, and strong mechanical properties (Feng *et al.,* 2019; Domagała *et al.,* 2020). CNTs can effectively combine with semiconductor nanoparticles to form nanocomposites with enhanced photocatalytic activity. Their incorporation improves charge separation, suppresses electron–hole recombination, enhances visible-light absorption, and facilitates electron transfer during photocatalytic reactions. In addition, the interaction between CNTs and CuO alters the electronic structure of the nanocomposite, improving its photocatalytic efficiency. Several studies have reported enhanced photocatalytic performance of CuO through doping with single-walled and multi-walled CNTs (Mahmoodi *et al.,* 2016; Sapkota *et al.,* 2020; Marques Neto *et al.,* 2017).

Photocatalytic nanocomposites have significant potential in wastewater treatment and environmental remediation. Their application contributes to several United Nations Sustainable Development Goals (SDGs), particularly SDG 6 (Clean Water and Sanitation) through water purification and pollutant removal, SDG 14 (Life Below Water) through protection of aquatic ecosystems, and SDG 9 (Industry, Innovation, and Infrastructure) through the development of sustainable and innovative treatment technologies.

Despite extensive research on CNT-based photocatalysts, limited studies have reported the preparation of CNT-based nanocomposites using CNTs grown on powdered activated carbon (PAC) at relatively low synthesis temperatures. This study presents the facile synthesis of pristine CNTs grown on PAC using chemical vapor deposition (CVD), followed by the preparation of a CuO/CNT nanocomposite through wet chemical impregnation at a relatively low temperature of 250 °C. The synthesized nanocomposite was characterized using FTIR, XRD, SEM-EDS, TEM, and TGA analyses. Its photocatalytic performance was evaluated for the degradation of Methyl Green (MG) and Methyl Orange (MO) dyes under visible-light irradiation. The effects of initial dye concentration, solution pH, catalyst dosage, oxidant concentration, reaction time, and degradation kinetics were systematically investigated. Furthermore, the use of an energy-efficient 6 W LED source instead of high-energy Hg or Xe lamps enhances the sustainability and cost-effectiveness of the proposed photocatalytic system.

MATERIALS AND METHOD

Materials used

Nickel (II) nitrate hexahydrate (98%) was purchased from Scharlau, Spain. Copper (II) nitrate trihydrate (98%) was obtained from Phillip Harris Education, UK. Methyl green was purchased from BioChemica, Germany, and Methyl orange from Merck, Germany. Powdered Activated Carbon (PAC), acetone (99.8%), and absolute ethanol (99.8%) were purchased from Fisher Scientific. Hydrogen, acetylene, and nitrogen gases were 99.9% pure. Aqueous solutions of methyl green and methyl orange with the requisite concentrations were prepared using deionized water.

Fabrication of CNT on PAC

p-CNT were produced via CVD technique on PAC impregnated with a nickel catalyst. A method called incipient wetness impregnation was applied to disperse the metallic catalyst on the surface of PAC (Al-Saadi *et al.,* 2011; Aljumaily *et al.,* 2018; Alayan *et al.,* 2018). PAC (3 g) was added to nickel (II) nitrate hexahydrate acetone solution with a 2 wt.% Ni (II) in a (2 cm diameter) glass vial. The mixture was sonicated at room temperature for 30 min, then dried at 100 ^{o}C until all the solvent evaporated. The dried cake of (Ni/PAC) catalyst-substrate was ground to a fine powder and then used for the growth of CNT by CVD through heat treatment steps. First, 200 mg of Ni/PAC substrate was placed in a ceramic boat and inserted inside a ceramic tube (65 mm OD, 60 mm ID, 1200 mm Length) in a tubular furnace. The Ni/PAC substrate was calcinated at 200 ^{o}C for 1 h under N_2(g) flow to get rid of moisture, followed by reduction by H_2(g) at the same temperature for 1 h. After that, the temperature was raised at 10 ^{o}C/min up to 650 ^{o}C under N_2(g) atmosphere. Then the N_2(g) flow was stopped and H_2(g) (400 mL/min) and C_2H_2(g) (60 mL/min) were allowed to flow for 30 min to start the reaction growth of CNT. When the reaction was terminated, the reaction gases were stopped and N_2(g) was delivered again to cool down the system to room temperature and to prevent oxidation of the produced CNT.

Preparation of CuO/CNT Nanocomposite

The CuO/CNT nanocomposite was prepared as follows. About 200 mg of prepared CNT was mixed with copper (II) nitrate trihydrate solution in ethanol in a 2% w/w Cu^{2+}/CNT ratio. The mixture was sonicated at room temperature for 30 min. Then it was dried in an oven at 80 ^{o}C to evaporate the solvent. The dried powder was further calcined at 250 ^{o}C under N_2(g) flow in a tubular furnace for 2h. Finally, the produced CuO/CNT nanocomposite was allowed to cool down to room temperature under N_2(g) flow to avoid oxidation of the sample.

Characterization of CuO/CNT

The produced CuO/CNT nanocomposite was investigated using different characterization techniques. Fourier Transform Infrared Spectroscopy (FTIR, Bruker, TENSOR 37) was used to study the surface nature of carbon material. The shape and morphology of the PAC/Ni, p-CNT, and CuO/CNT nanocomposite were identified by scanning electron microscope (JSM-6510LA) under an accelerating voltage of 20 kV and by transmission electron microscope (JEOL, JEM-1400) at 120 kV. The chemical element composition was also determined through an energy dispersive spectroscopy EDS (JED-2300). Powder X-ray diffraction analysis of the p-CNT and CuO/CNT nanocomposite was carried out using a D8 Discover Bruker X-ray diffractometer with Cu Ka radiation (k= 1.5418 Å) operating at 40 kV and 40 mA with 2θ ranging from 10 to 80 degrees, increment 0.02°. Thermal gravimetric analysis (TGA, SDT Q600, TA Instruments, USA) was performed under airflow (50 mL/min) from ambient to 1000 ^{o}C at a heating rate of 10 ^{o}C/min to study the thermal stability of produced materials.

CuO/CNT Catalyst Performance

The photocatalytic activity of the developed CuO/CNT nanocomposite catalyst was investigated by studying the removal efficiency of MG and MO from aqueous solution through CuO/CNT. Experiments were performed in a batch photoreactor. Different parameters have been studied including the effect of catalyst dose, initial dye concentration, contact time, oxidant concentration, and pH of the solution on photocatalytic dye degradation. To investigate the effect of catalyst dose and determine the optimum amount of catalyst, different amounts of CuO/CNT (5, 10, 30, and 50 mg) were mixed with 50 mL of dye solution (10 ppm) in the presence of H_2O_2 (3 mM, 1 mL). The solutions were stirred for 30 min in the dark to balance the adsorption and desorption of dye on the surface of the catalyst. Then the solutions were irradiated with a visible light LED lamp (6 W, 60 Hz) to initiate photocatalytic reactions. Samples were withdrawn from each solution at certain time intervals for 180 min. The catalyst was separated from the mixture by centrifugation at 4000 rpm for 20 min. Finally, the absorbance of clear solutions was measured by a UV-visible spectrophotometer (Agilent, Cary 100) at the maximum wavelength of dyes (464 nm for MO and 630 nm for MG). The effect of initial dye concentration on photocatalysis experiments was also studied. 50 mL solutions with different dye concentrations (10, 15, and 20 ppm) and H_2O_2 (3 mM) were mixed with 10 mg CuO/CNT catalyst. The effect of solution pH was investigated by using four pH values (3, 5, 7, and 9). After maintaining the pH of each dye solution (10 ppm, 50 mL with H_2O_2, 3 mM), 10 mg catalyst was added to them. To study the effect of time, 10 mg catalyst was mixed with 50 mL dye solution (10 ppm) with H_2O_2, 3 mM. The effect of oxidant concentration was also investigated by using four different H_2O_2 concentrations (1, 3, 5, and 7 mM) with a fixed oxidant volume in each experiment of 1 mL.

RESULTS AND DISCUSSION

Surface Characterization of CuO/CNT

FTIR spectroscopy was used to investigate the surface characteristics and functional groups present on the synthesized CNT/CuO nanocomposite. Fig. 1 presents the FTIR spectrum of CNT/CuO, highlighting the major functional groups and Cu–O bonding vibrations. The peak

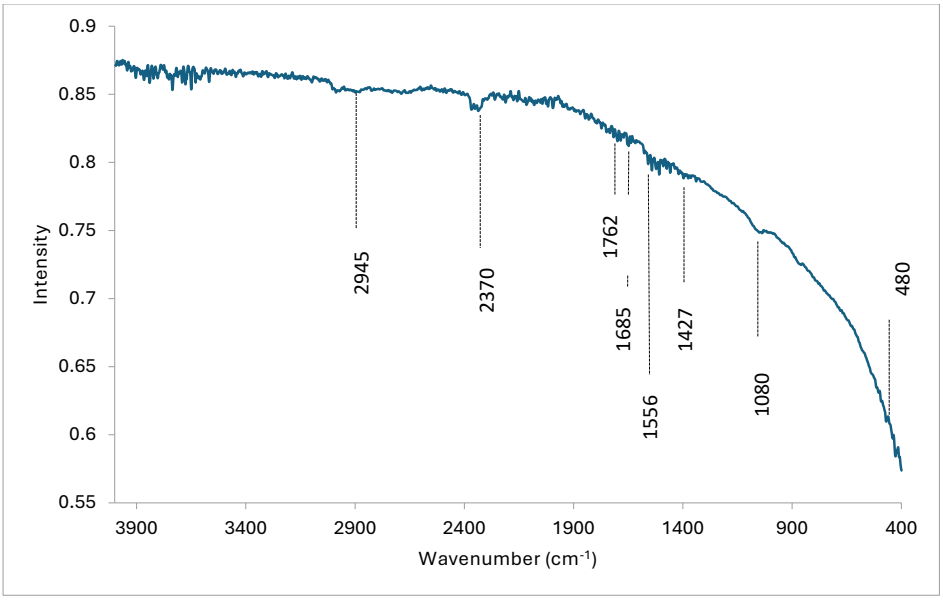

Fig. 1. FTIR spectrum of CuO/CNT nanocomposite

at 2945 cm^{-1} corresponds to –CH and CH_2 stretching vibrations. The band around 2370 cm^{-1} is attributed to adsorbed CO_2 (Aljumaily et al., 2018). The absorption bands in the range of 1400–1762 cm^{-1} indicate the presence of oxygen-containing functional groups, mainly associated with C=O stretching vibrations of carboxylic and carbonyl groups. In addition, the peaks at 1556 and 1685 cm^{-1} are assigned to C=C skeletal stretching vibrations. The band at 1427 cm^{-1} corresponds to the symmetric stretching of C=O groups, while the peak at 1080 cm^{-1} represents C=O vibrations of various oxygen-containing functional groups. Furthermore, the characteristic peak observed at 480 cm^{-1} confirms the presence of Cu–O bonding, indicating the successful incorporation of CuO nanoparticles onto the CNT surface, as most metal oxides absorb within the 400–1000 cm^{-1} region (Mahmoodi et al., 2016; Alayan et al., 2019).

Morphological Characterization of CuO/CNT Nanocomposite

The structural morphology of PAC impregnated with a nickel catalyst is presented in Fig. 2(a–c), which illustrates the surface texture, catalyst dispersion, and elemental composition of the prepared material. The SEM images reveal that PAC possesses a rough and irregular porous structure. The Ni catalyst was successfully impregnated and uniformly dispersed on the PAC surface, as observed in the SEM and TEM images of PAC/Ni shown in Fig. 2(a, b). The high porosity and large surface area of PAC promoted effective catalyst distribution and minimized the agglomeration of catalyst particles on the carbon support surface. This observation was further supported by the EDS analysis presented in Fig. 2(c), which confirmed that the sample contained 95.5 wt% carbon, 2 wt% oxygen, and approximately 1.53 wt% nickel.

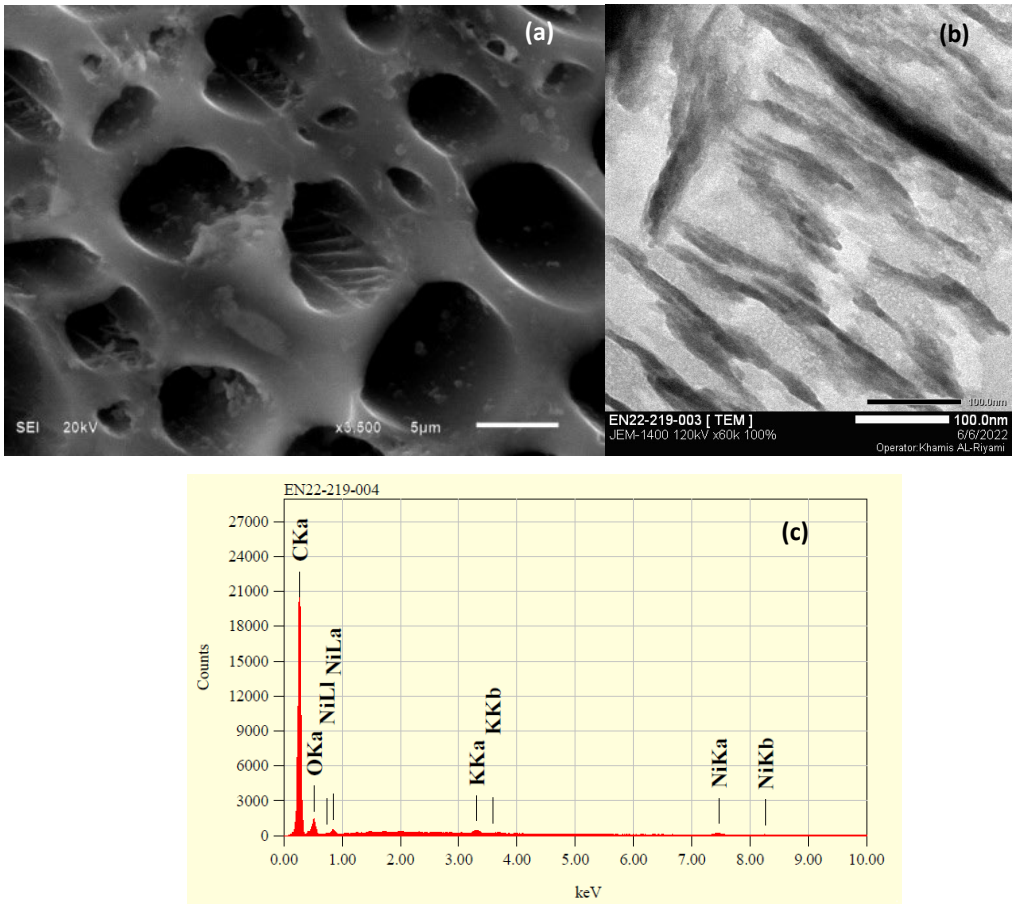

Fig. 2. (a) SEM, (b) TEM, (c) EDS of PAC impregnated with Ni(II) catalyst

Figure. 3(a, b) illustrates the morphology of p-CNT grown on PAC, highlighting the formation of interconnected carbon nanotube networks. The SEM and TEM images show a tube-like morphology with diameters ranging from 50 to 120 nm, forming a net-like structure. Figure 4(a–d) presents the morphology of the synthesized CuO/CNT nanocomposite and the distribution of CuO nanoparticles on the CNT surface. The CuO/CNT nanocomposite retained a similar CNT morphology, while CuO nanoparticles formed clusters surrounding the carbon nanotubes, with particle diameters ranging from 7 to 12 nm.

Structural Characterization of CuO/CNT Nanocomposite

Figure. 5 presents the XRD patterns of p-CNT and the synthesized CuO/CNT nanocomposite, highlighting the crystalline structure of CNT and the successful incorporation of CuO nanoparticles. The diffraction peaks of CNT observed at 26.72° and 43.3° correspond to the graphitic (002) and (111) planes, respectively, confirming the graphitic nature of the synthesized CNTs (Mahmoodi et al., 2016). The peak located at 20.98° may be attributed to the disordered stacking of the nanotube layers. In addition, the appearance of a shoulder peak at 27.13° could be associated with the presence of nickel, which is consistent with the elemental composition shown in Fig. 3(c).

The XRD pattern of the CuO/CNT nanocomposite shown in Fig. 5 further demonstrates the

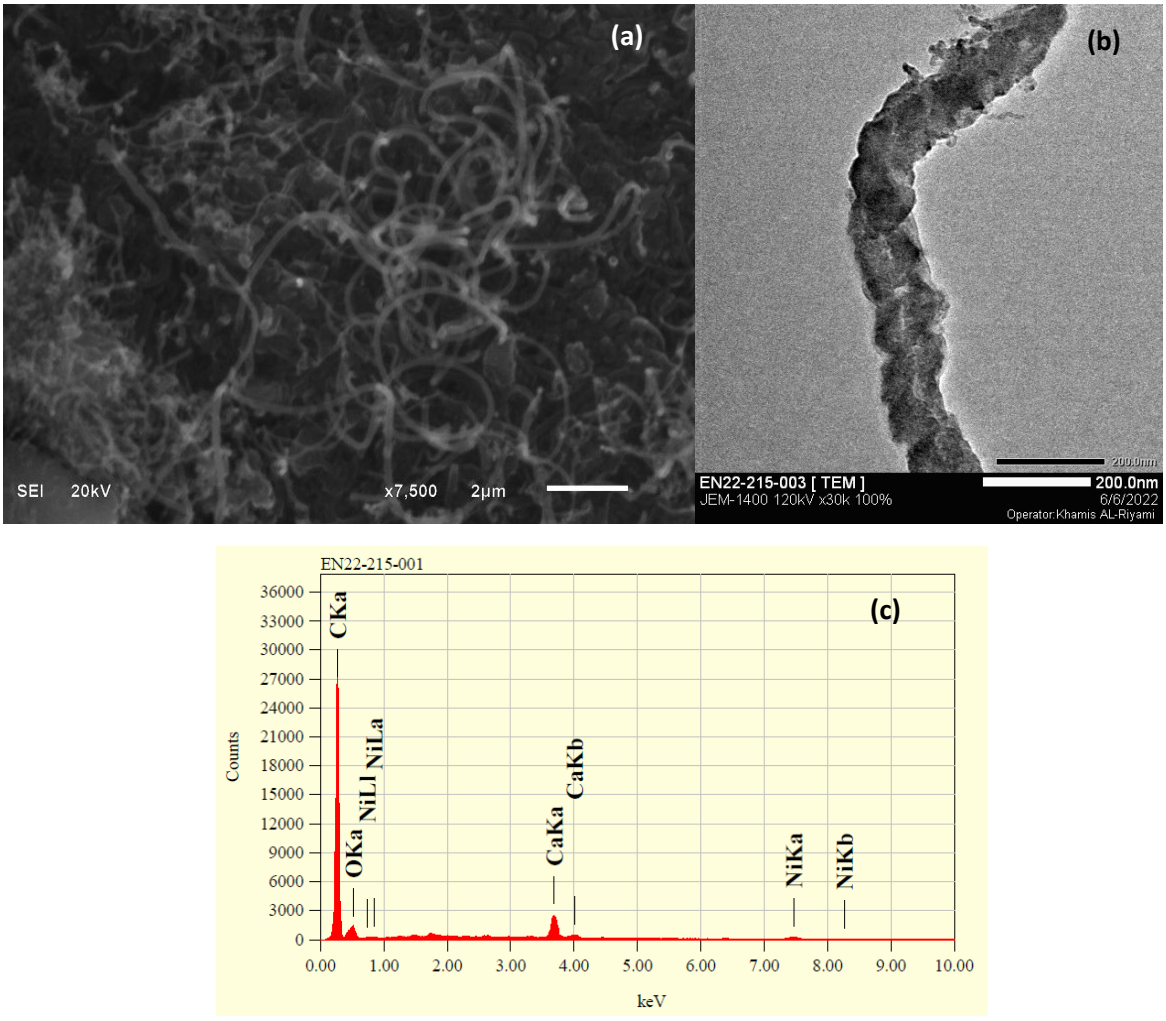

Fig. 3. (a) SEM, (b) TEM, (c) EDS of p-CNT

formation of crystalline CuO phases after calcination. Additional diffraction peaks appearing at 35.5°, 38.8°, 50.8°, and 68.2° are characteristic of CuO (JCPDS #00-048-1548; JCPDS #005-0661), corresponding to the lattice planes of (002), (−111), (111), and (220), respectively. The graphitic carbon peaks remained at the same positions after calcination and CuO incorporation, indicating that the CNT structure remained stable and was not reduced during the calcination process (Mahmoodi et al., 2016). Similar observations have also been reported in previous studies (Wu et al., 2002; Ping and An-juan, 2016; Dana and Sheibani, 2021).

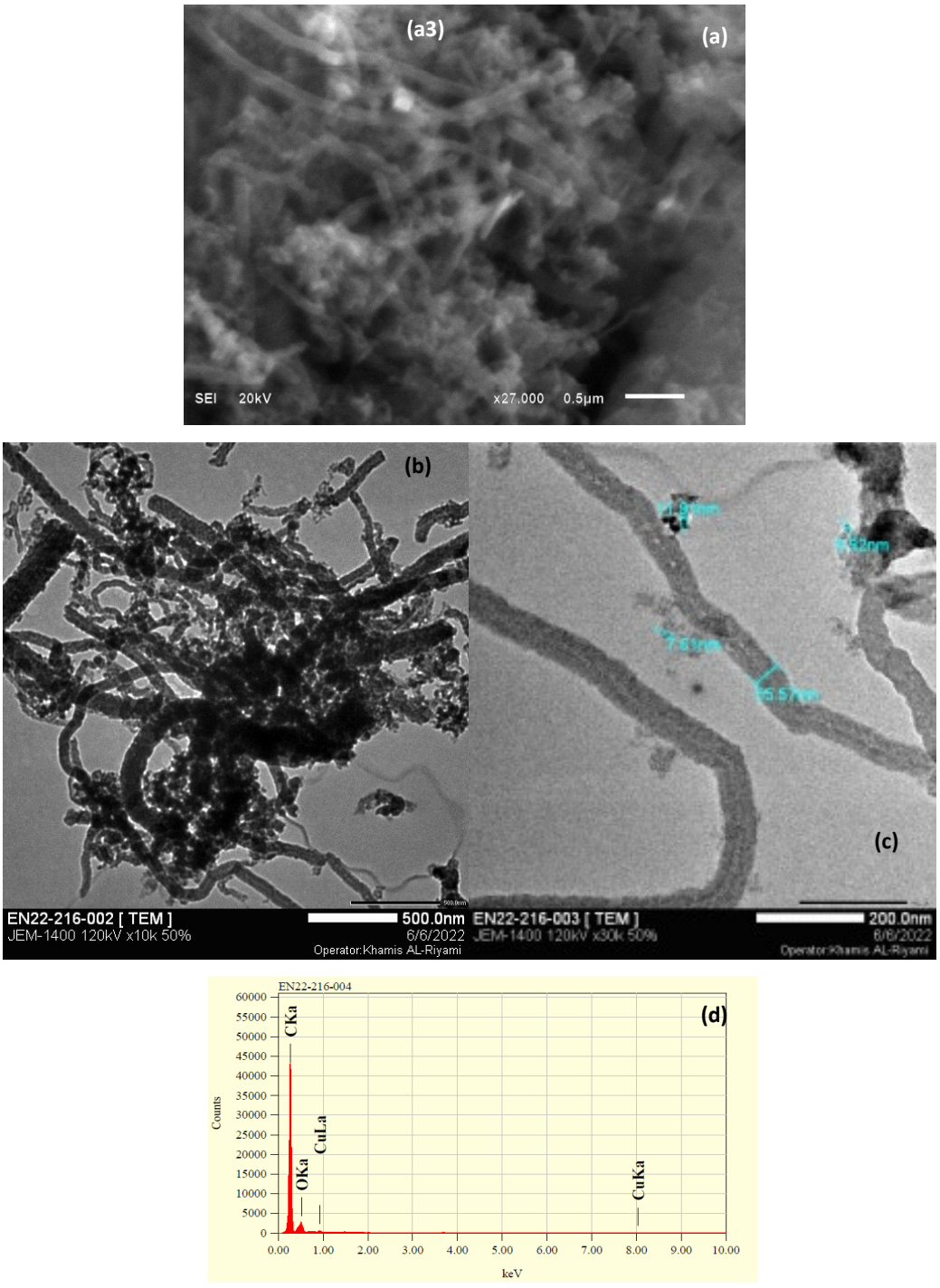

Fig. 4. (a) SEM, (**b, c**) TEM, (**d**) EDS of CuO/CNT nanocomposite

Thermal Properties of CuO/CNT Nanocomposite

Thermogravimetric analysis (TGA) was performed to evaluate the thermal stability and oxidation behavior of the synthesized materials. Figure. 6 presents the TGA and derivative weight curves of PAC, PAC-Ni, p-CNT, and CuO/CNT, illustrating their degradation patterns, oxidation onset temperatures, and residual mass after thermal decomposition. All samples exhibited a single-step degradation behavior. The oxidation onset temperatures of PAC, PAC-Ni, p-CNT, and CuO/CNT were approximately 445, 432, 566, and 461 °C, respectively. These temperatures correspond to the points at which significant weight loss begins and are also associated with the peaks observed in the derivative weight curves (Fig. 6).

The degradation of PAC and PAC-Ni started at nearly 375 and 355 °C, respectively, resulting in an overall weight loss of about 70%. The relatively low decomposition temperatures of these

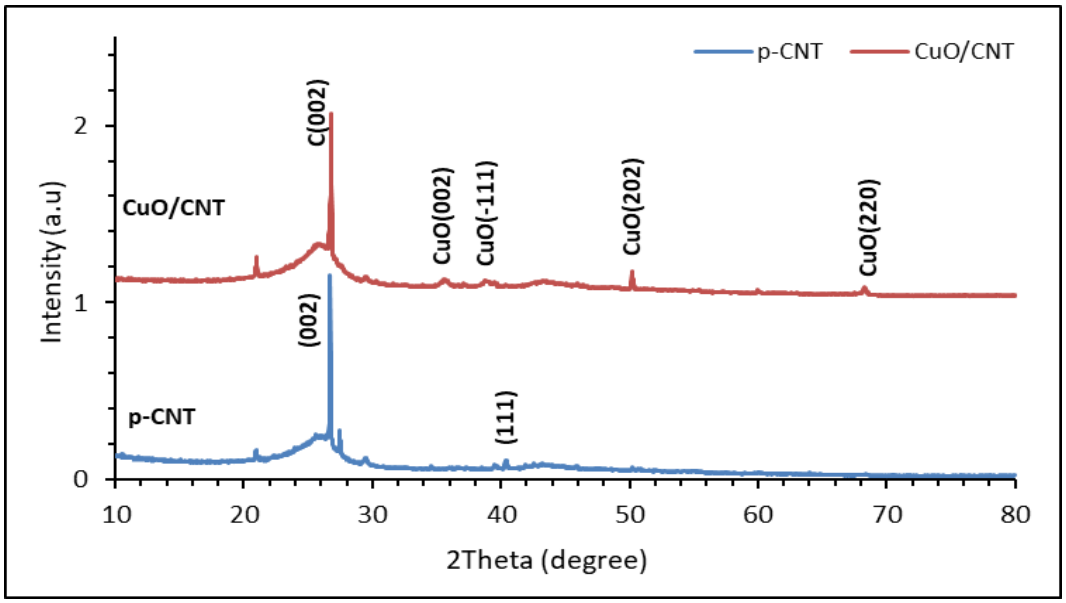

Fig. 5. XRD patterns of p-CNT and CuO/CNT nanocomposite

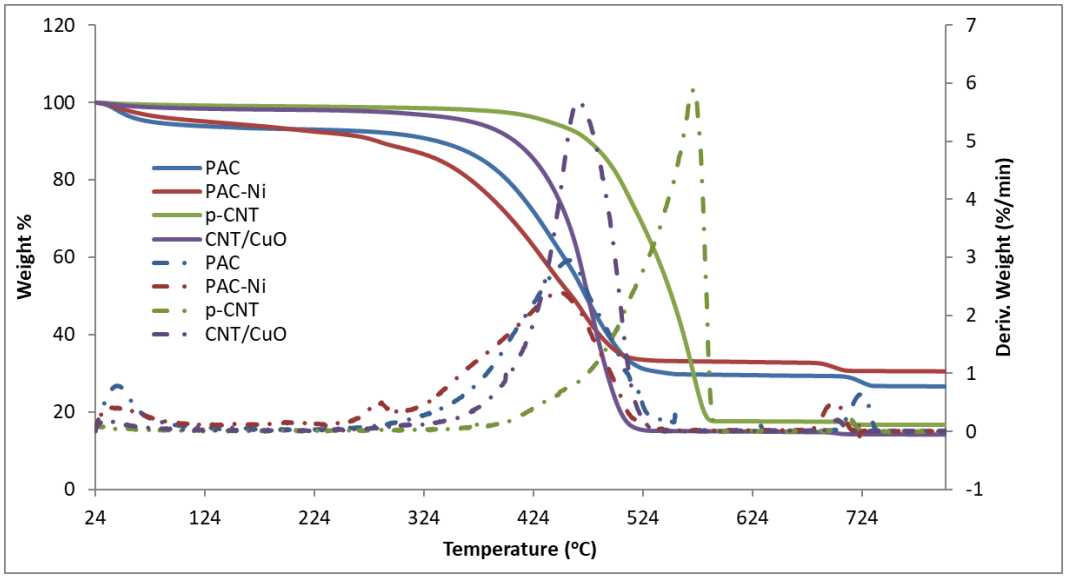

Fig. 6. TGA and DTG of PAC, PAC-Ni, p-CNT and CuO/CNT

materials are attributed to the presence of amorphous carbon and thermally sensitive oxygen-containing functional groups, as confirmed by the FTIR analysis (Datsyuk et al., 2008). In contrast, p-CNT exhibited significantly higher thermal stability, with an oxidation temperature of approximately 566 °C. The weight loss percentages of p-CNT and CuO/CNT were around 80%. The sharp mass reduction observed above 500 °C is mainly associated with the oxidation of amorphous carbon and residual metal impurities, which accelerate CNT oxidation through exothermic reactions and enhanced heat transfer (Aljumaily et al., 2018; Alayan et al., 2018; Alayan et al., 2019).

Figure. 6 also shows the variation in residual mass after thermal decomposition, reflecting compositional changes during catalyst impregnation and CNT growth. The residual mass of PAC was approximately 26%, mainly due to impurities present in the carbon substrate. After nickel catalyst impregnation, the residual mass increased to about 30%. However, the residual mass decreased to nearly 16% and 14% for p-CNT and CuO/CNT, respectively, which may be attributed to the formation of new nanostructures on the catalyst surface and changes in the overall material composition.

The TGA results further confirmed the successful formation of CuO nanoparticles on CNTs. As shown in Fig. 6, the oxidation onset temperature of CuO/CNT shifted from 566 °C for pristine CNT to 461 °C after CuO incorporation, indicating that CuO significantly catalyzed the oxidation of CNTs. The faster oxidation of CuO/CNT compared to p-CNT is attributed to heat localization around CuO particles, which enhances heat transfer and accelerates the oxidation process. These findings are consistent with the SEM, TEM, and XRD analyses and are in agreement with previous studies reported by Manasrah et al. (2018).

Photocatalytic Studies of CuO/CNT

The photocatalytic performance of the fabricated CuO/CNT nanocomposite was examined through the degradation of MG and MO in aqueous solutions, and the effects of different parameters were studied.

Effect of Contact Time

The time-dependent photocatalytic degradation behavior of Methyl Green (MG) and Methyl Orange (MO) under visible-light irradiation using 10 mg of CuO/CNT catalyst is presented in Fig. 7(a–d). Figure 7(a, b) illustrates the changes in the UV–Vis absorbance spectra of MG and MO solutions during irradiation, while Fig. 7(c) visually demonstrates the discoloration of the dye solutions with increasing irradiation time. Figure 7(d) summarizes the degradation efficiency of both dyes as a function of reaction time.

When 10 ppm solutions of MG and MO were irradiated under visible light for 180 min in the presence of 10 mg of CuO/CNT catalyst, the absorbance of MG decreased significantly from 0.45 at t = 0 min to 0.04 at t = 180 min, indicating a much higher degradation efficiency compared to MO, as shown in Fig. 7(a, b). The discoloration of the dye solutions was also visually evident in Fig. 7(c), confirming the photocatalytic activity of the synthesized nanocomposite.

As shown in Fig. 7(d), the degradation rate was rapid during the initial stages of irradiation, particularly within the first 30 min for MG and 50 min for MO, as indicated by the sharp increase in degradation percentage. Subsequently, the degradation rate gradually slowed and approached a steady state after nearly 120 min. This behavior may be attributed to the progressive occupation of active sites on the CuO/CNT surface by dye molecules, leading to surface saturation and reduced adsorption capacity. The initial rapid photodegradation is mainly due to the abundance of available active sites on the catalyst surface, whereas the slower degradation rate at later stages results from the reduced availability of these active sites as the reaction proceeds (Dana

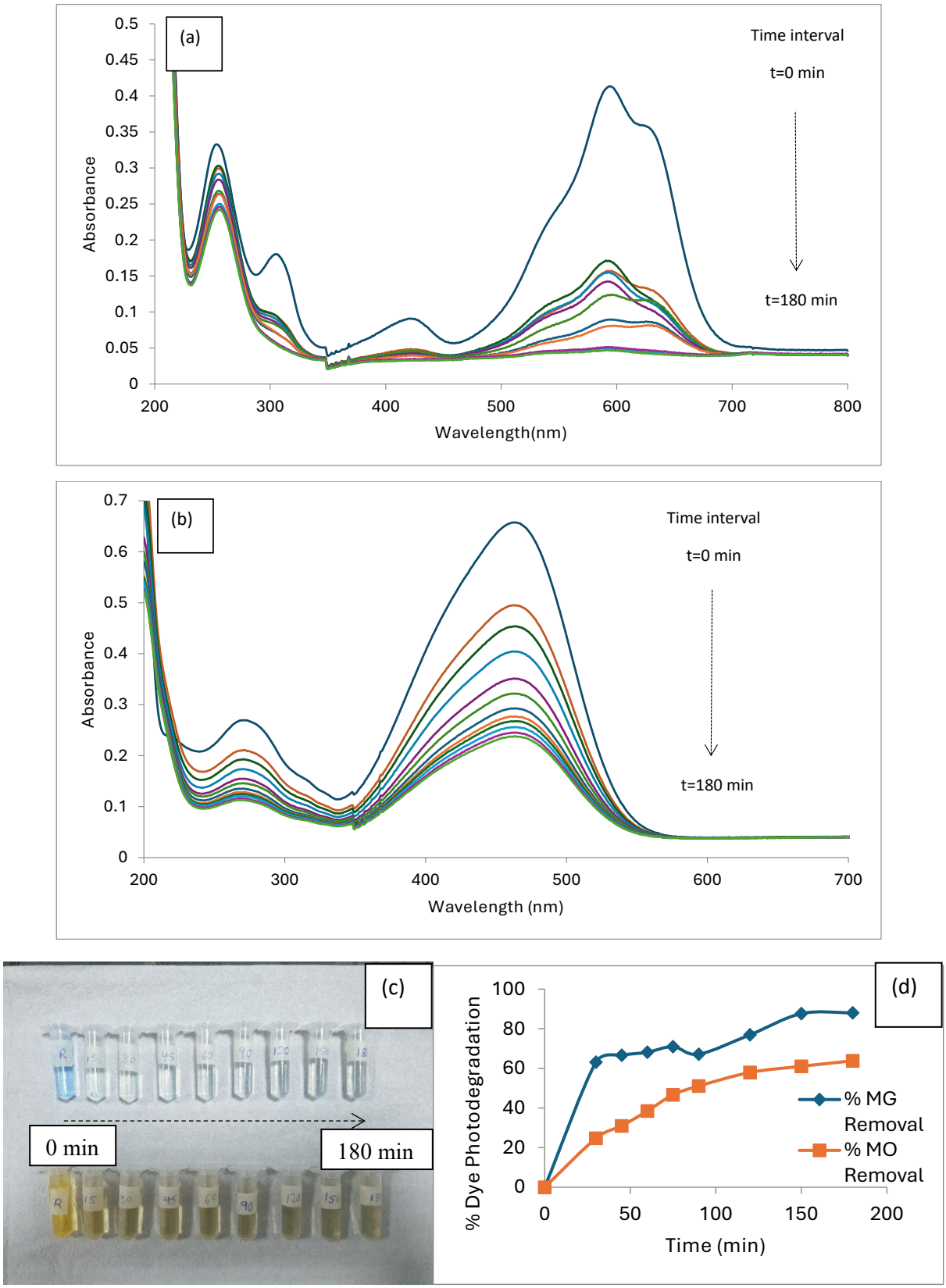

Fig. 7. (a) UV-Vis spectra of photodegradation of MG and MO, **(b)** dye solutions at different time intervals in the presence of CuO/CNT, **(c)** decolorization process of MG and MO dye solutions, and **(d)** Effect of time of photocatalysis on % Dye degradation for MG and MO

and Sheibani, 2021). Similar behavior for MG degradation has also been reported by Kumar et al. (2017) using $Ni_{0.10}La_{0.05}TiO_2$ photocatalysts.

Effect of Catalyst Dosage

Figure 8 illustrates the effects of catalyst dosage and initial dye concentration on the photocatalytic degradation efficiency of MG and MO using the CuO/CNT nanocomposite under visible-light irradiation. Figure 8(a) presents the influence of CuO/CNT dosage on dye degradation, while Fig. 8(b) shows the variation in degradation efficiency with changes in the initial dye concentration.

As shown in Fig. 8(a), the degradation efficiency of both dyes increased with increasing catalyst dosage up to an optimum level. This enhancement in photocatalytic activity can be attributed to the increased availability of active sites on the catalyst surface, which promotes

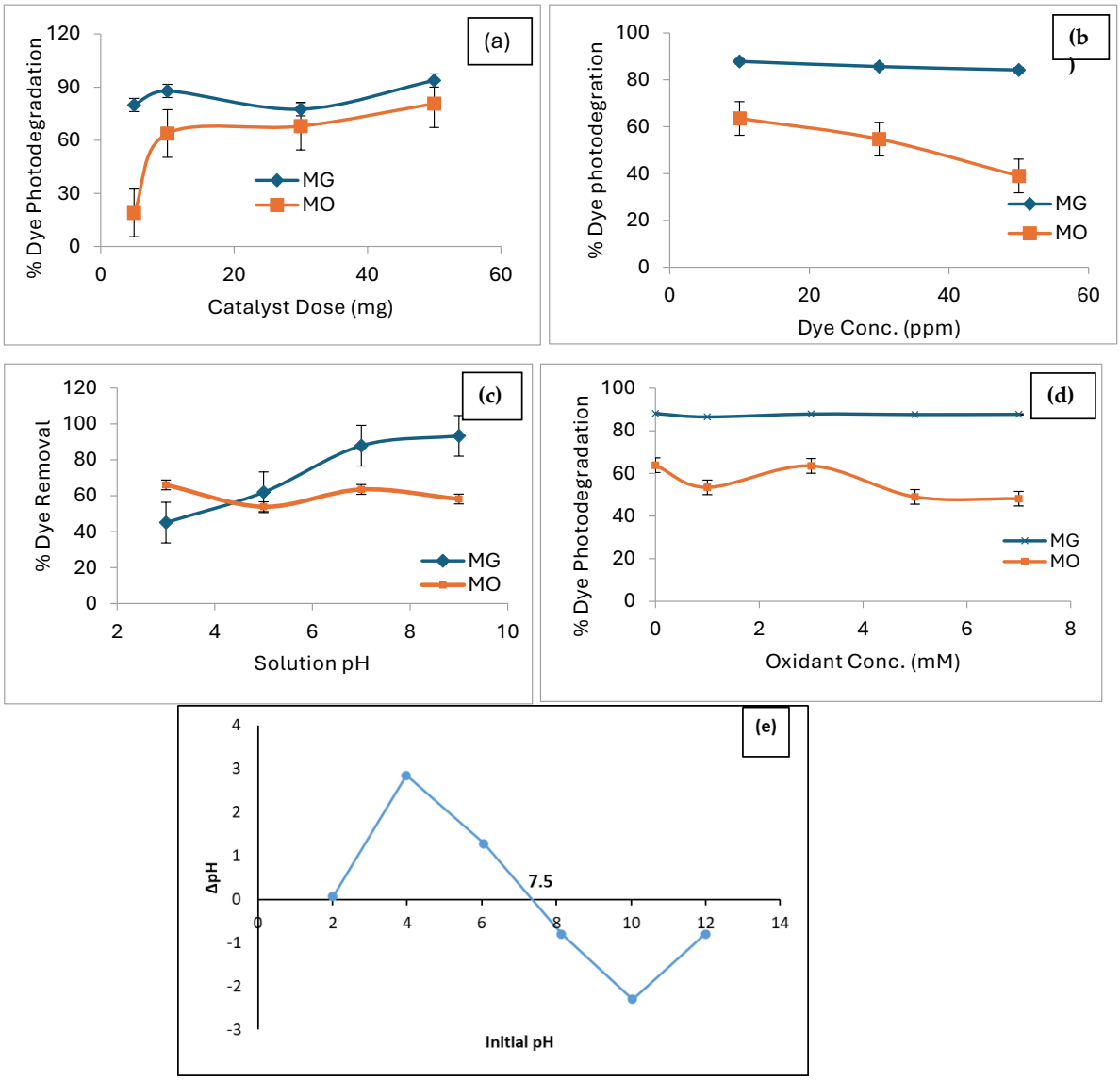

Fig. 8. **(a)** Effect of the amount of CuO/CNT photocatalyst, **(b)** Effect of initial dye concentration, **(c)** Effect of pH of dye solution, and **(d)** Effect of oxidant concentration on % Dye removal of methyl green and methyl orange **(e)** point of zero charge (pzc) of CuO/CNT

the generation of reactive free radicals responsible for dye degradation. In addition, a higher catalyst dosage increases the adsorption of dye molecules onto the CuO/CNT surface, thereby supporting the photocatalytic process. However, beyond the optimum dosage, fluctuations in degradation efficiency were observed. This behavior may be due to increased turbidity in the solution caused by excessive catalyst loading, which reduces light penetration and limits photocatalytic activity (Mahmoodi et al., 2016; Kumar and Pandey, 2017). Therefore, 10 mg of catalyst was selected as the optimum dosage in this study to minimize turbidity effects while maintaining high degradation efficiency. Under these conditions, the degradation efficiencies reached approximately 88% for MG and 63% for MO.

Figure 8(b) demonstrates the effect of initial dye concentration on the degradation efficiency of MG and MO. MG (blue curve) maintained relatively high degradation efficiency, decreasing only slightly from approximately 88% at 10 ppm to 84% at 50 ppm, indicating that the CuO/CNT photocatalyst remained effective even at higher MG concentrations. In contrast, MO (red curve) exhibited a significant decline in degradation efficiency, decreasing from approximately 63% at 10 ppm to 38% at 50 ppm. The larger error bars observed at higher concentrations suggest increased variability in the degradation process, possibly due to mass-transfer limitations and reduced reaction efficiency.

The decrease in degradation efficiency with increasing dye concentration can be attributed to several factors. At higher dye concentrations, excessive dye molecules in the solution hinder the penetration of incident light to the catalyst surface, thereby reducing the formation of reactive oxidizing species required for effective photocatalysis. Furthermore, a large number of dye molecules can adsorb onto the catalyst surface and block active sites responsible for generating hydroxyl radicals (OH•), resulting in a lower availability of reactive species for dye degradation (Khan et al., 2024). Consequently, the overall photodegradation percentage decreases with increasing dye concentration (Kumar, 2017; Kumar and Pandey, 2017). Similar observations were reported by Rashed et al. (2007), who found that increasing MO concentration reduced its degradation efficiency. Comparable trends have also been widely reported for the photocatalytic degradation of organic pollutants (Reza et al., 2017; Avasarala et al., 2010).

Effect of pH of the solution

The pH of the aqueous solution plays a crucial role in the photocatalytic process because it influences both the surface charge of the catalyst and the electrostatic interactions between the catalyst and dye molecules. Figure 8(c) illustrates the effect of solution pH on the photodegradation efficiency of MG and MO, while Fig. 8(e) presents the point of zero charge (pzc) of the CuO/CNT catalyst.

As shown in Fig. 8(c), the photocatalytic degradation efficiency of MG increased significantly with increasing pH. The degradation efficiency reached approximately 93% at pH 9, compared to 88% at neutral pH, and decreased to 62% and 45% under acidic conditions at pH 5 and 3, respectively. In contrast, MO degradation exhibited an opposite trend. The degradation efficiency decreased from 66% at pH 3 to 53% at pH 5, followed by a slight increase to 58% at pH 9. These variations indicate that the photocatalytic behavior of CuO/CNT strongly depends on the electrostatic interactions and adsorption characteristics governed by the solution pH.

Figure 8(e) shows that the point of zero charge (pzc) of CuO/CNT is approximately 7.5, indicating that the catalyst surface is positively charged below this pH and negatively charged above it (Sharifpour et al., 2022). The substantial increase in MG degradation with increasing pH can therefore be explained by changes in the surface charge of the catalyst. At very low pH, the positively charged CuO/CNT surface strongly repels the cationic MG dye molecules, resulting in lower degradation efficiency. As the pH increases, the catalyst surface gradually

becomes negatively charged, enhancing the electrostatic attraction between the catalyst and MG molecules and thereby improving adsorption and photocatalytic degradation. In alkaline conditions, the abundance of OH^- ions further enhances photocatalytic activity by promoting the formation of hydroxyl radicals (OH•) through reactions with photogenerated holes, which play a major role in dye degradation.

In contrast, the degradation efficiency of the anionic MO dye decreased under alkaline conditions due to electrostatic repulsion between the negatively charged catalyst surface and negatively charged MO molecules. Additionally, OH^- ions may compete with MO molecules for adsorption sites on the catalyst surface, thereby reducing photocatalytic efficiency. Similar pH-dependent photocatalytic behavior has been reported for the degradation of organic pollutants using transition metal oxide catalysts (Sharifpour et al., 2022; Ma et al., 2018). This trend is clearly demonstrated in Fig. 8(c).

Effect of Oxidant Concentration

The effect of H_2O_2 concentration on the photocatalytic degradation efficiency of MG and MO was investigated in the concentration range of 1–7 mM using a fixed H_2O_2 volume of 1 mL. Figure 8(d) illustrates the variation in dye degradation efficiency with increasing H_2O_2 concentration under visible-light irradiation in the presence of the CuO/CNT photocatalyst.

As shown in Fig. 8(d), the degradation efficiency of MG remained nearly constant with increasing H_2O_2 concentration, indicating that the addition of excess oxidant had minimal influence on MG degradation. In contrast, MO degradation exhibited a slight decrease from approximately 63% at 1 mM H_2O_2 to 58% at 3 mM, followed by a small increase to about 60% at 5 mM before reaching a nearly stable condition. This behavior suggests that the effect of H_2O_2 concentration is closely related to the generation and consumption of reactive hydroxyl radicals (•OH) during the photocatalytic process.

At low H_2O_2 concentrations (1 mM), the oxidant enhances the production of hydroxyl radicals, thereby improving photocatalytic degradation efficiency. However, at higher concentrations (≥3 mM), excess H_2O_2 acts as a scavenger for hydroxyl radicals, reducing the number of highly reactive species available for dye degradation and forming less reactive intermediates such as HO_2• radicals (Youssef et al., 2016). In addition, the limited number of active sites available on the catalyst surface may contribute to the stabilization or slight decline in degradation efficiency observed at higher H_2O_2 concentrations. As a result, MO degradation slightly decreased, whereas MG degradation remained relatively stable (Hameed and Lee, 2009). Similar trends regarding the influence of H_2O_2 dosage on photocatalytic degradation have also been reported in previous studies (Youssef et al., 2016; Hameed and Lee, 2009).

Kinetics study of Photodegradation of MG and MO

The kinetic studies were conducted to determine the degradation rate of the organic dyes under the optimum conditions. The following equation was used:

$$\ln(C/C_o) = -kt \quad (1)$$

Where, C and C_o are the dye concentration at time t and at time = 0, respectively, k is the rate constant and t is the time in minutes.

The results of kinetic studies of photodegradation of MG and MO are shown in Fig.9 and Fig.10. The slope of the graph revealed the order of the reaction. The rate of photocatalysis degradation kinetics of MG and MO on CuO/CNT followed the pseudo-first-order kinetics model with a rate constant of 0.0081 and 0.005 min^{-1} for MG and MO, respectively. According to

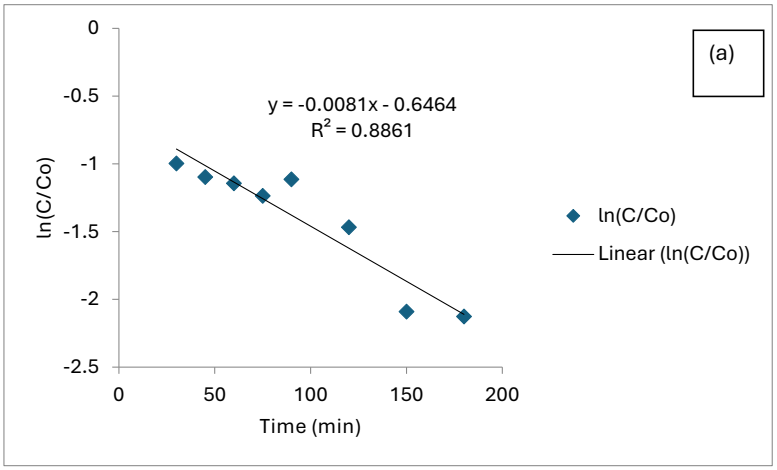

Fig. 9. The kinetics of photocatalytic degradation of MG on CuO/CNT

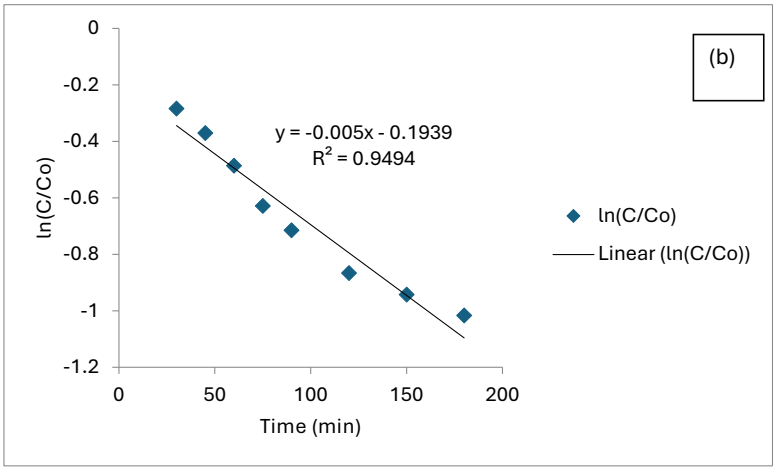

Fig. 10. The kinetics of photocatalytic degradation of MO on CuO/CNT

these results, CuO/CNT nanocomposite has shown excellent photocatalytic efficiency towards the photodegradation of both dyes. A similar rate constant of 0.00442 min^{-1} was obtained by Nesaraj *et al.* (2014) for the photodegradation of MO on CO_3O_4.

Mechanism of Photocatalytic Degradation

When a photocatalyst is irradiated with light of the same or higher energy than that of its band gap, electrons are excited from the valence band to the conduction band generating electron-hole pairs (Nesaraj, 2014). The generated electrons and holes will initiate the photodegradation process by participating in redox reactions. Dye degradation is facilitated by hydroxyl radicals, which are considered powerful, non-selective oxidants and can be generated from different reactions such as hydrogen peroxide decomposition, and the reaction of photogenerated holes with hydroxide anion and water molecules. Photodegradation of dyes can be summarized by the following reactions (Mahmoodi *et al.,* 2016):

$$\text{Photocatalyst} + h\nu \rightarrow \text{photocatalyst} (e_{CB}^{-} + h_{VB}^{+}) \quad (2)$$

$$h_{VB}^{+} + H_2O \rightarrow H^{+} + \cdot OH \quad (3)$$

$h_{VB}^{+} + OH^{-}$ à $\cdot OH$ (4)

$e_{CB}^{-} + O_2$ à $O_2^{\cdot -}$ (5)

$O_2^{\cdot -} + H^{+}$ à $HO_2^{\cdot}$ (6)

Dye + $\cdot OH$ à degradation products (7)

Dye + h_{VB}^{+} à oxidation products (8)

Dye + e_{CB}^{-} à reduction products (9)

The photogenerated electron-hole pairs can recombine in the absence of electron scavengers, releasing stored energy instantly; however, this recombination can be suppressed in the presence of molecular oxygen. Molecular oxygen plays a crucial role by capturing photogenerated electrons and reducing them to superoxide ion radicals.

The incorporation of carbon-based materials in photocatalysts enhances photocatalytic efficiency due to their cost-effectiveness, high availability, excellent adsorption capacity, and high porosity. In particular, carbon nanotubes (CNTs) in a nanocomposite photocatalyst significantly improve dye photodegradation by forming heterojunctions with CuO nanoparticles, as illustrated in Fig. 11. Photogenerated electrons in the conduction band of CuO are efficiently transferred to CNTs through the CuO/CNT heterojunction, where CNTs act as electron acceptors and conductive pathways. This electron migration suppresses electron–hole recombination by spatially separating charge carriers. Meanwhile, the photogenerated holes remain in the valence band of CuO and participate in oxidation reactions, leading to the formation of reactive oxygen species. The synergistic interaction between CuO and CNTs significantly enhances the photocatalytic degradation of MG and MO dyes (Sapkota *et al.,* 2020; Aroob *et al.,* 2023). Furthermore, CNTs facilitate rapid electron transport and oxygen activation, thereby improving overall photocatalytic efficiency (Mahmoodi *et al.,* 2016).

Comparison of CuO/CNT photocatalytic performance with previous studies

The comparison of obtained results for the photocatalytic degradation of MG and MO with previous studies emphasizes the efficiency of the CuO/CNT catalyst produced by the CVD

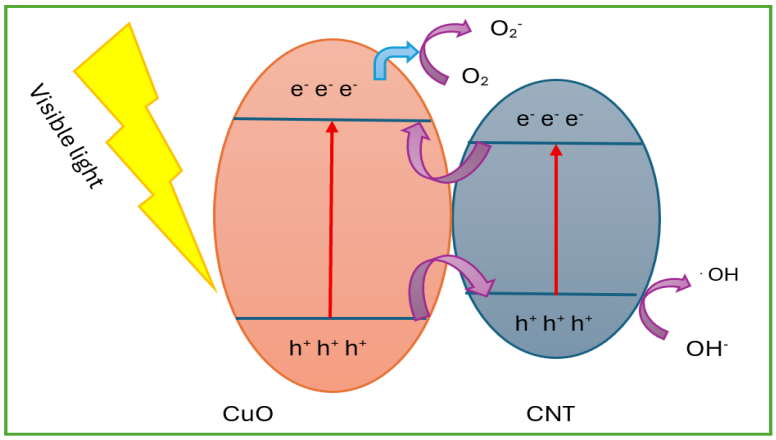

Fig. 11. Illustrated mechanism of generation of reactive oxygen species and hydroxyl free radicals due to irradiation of CuO/CNT nanocomposite with visible light

Table 1. Comparison of photocatalytic performance of CuO/CNT with literature for degradation of MG and MO

Catalyst	Dye	Synthesis Method	Catalyst dose	Light Source	Degradation (%); time (min)	Kinetic Model/rate constant	Reference
CuO/CNT	MG	CVD + Impregnation Calcination Temp 250 °C	2 wt.%	LED (6 W)	90%; 180min	Pseudo-first-order $0.0081 min^{-1}$	This work
CuO/CNT	MG	Impregnation Calcination Temp 300 °C	3 wt.%	Hg Lamp	78% 240min	Pseudo-first-order 0.0062	(Mahmoodi *et al.,* 2016)
CuO	MG	Green Synthesis Calcination Temp 400 °C	-	UV Lamp	65.2%; 240min	First-order 0.0044	(Aroob *et al.,* 2023)
CuO/CNT	MB	Sol-Gel Calcination Temp 450 °C	5 wt.%	Xe Lamp	85%; 180min	Pseudo-first-order	(Sapkota *et al.,* 2020)
CuO/Al_2O_3	MO	microwave-assisted thermal decomposition route Calcination Temp 1000 °C	2g/L	UV	94.2%; 180min	Not reported	(Alhussain *et al.,* 2024)

and impregnation techniques, as shown in Table 1. The nanocomposite synthesized at low calcination temperature (250 °C) resulted in 90% degradation of MG with merely 2 wt.% CuO unlike other reports (Mahmoodi *et al.,* 2016; Sapkota *et al.,* 2020; Ma *et al.,* 2018; Dana and Sheibani, 2021; Aroob *et al.,* 2023; Alhussain *et al.,* 2024) requires greater CuO loadings (e.g., 3–5 wt.%), and elevated calcination temperatures (300–450°C) for synthesis. No studies were found to be available on photocatalytic degradation of MO using CuO/CNT. Furthermore, this method is more sustainable as the use of an energy-efficient LED light (6 W) contrasts with the dependence on high-energy-consuming Hg and Xe lamps. These results confirm that the synthesis method applied in this work improves photocatalytic efficiency while preserving reduced energy consumption and cost-effectiveness, therefore favoring it for wide-scale applications.

CONCLUSION

CuO/CNT, a novel nanocomposite photocatalyst, was successfully synthesized using PAC through the CVD technique, followed by a simple impregnation process and calcination. Characterization techniques including XRD, SEM, EDS, TEM, and TGA confirmed the formation of CuO nanoparticles on the CNT surface. XRD patterns verified the presence of crystalline CuO particles along with graphitic CNTs. TGA results further supported the formation of CuO nanoparticles. This was evidenced by the shift in oxidation onset temperature from 566 °C for undoped CNTs to 461°C for CuO/CNT.The photocatalytic performance of CuO/CNT was evaluated through the degradation of MG and MO dyes in aqueous solutions. The nanocomposite achieved 90% removal of MG and 67% removal of MO, both in the presence and absence of H_2O_2.The use of nanocomposites for photocatalytic degradation contributes to several Sustainable Development Goals (SDGs). These include promoting clean water, reducing environmental pollution, combating climate change, and encouraging innovation for sustainable industries.Overall, the results indicate that CuO/CNT is a promising photocatalytic nanocomposite. It can be synthesized effectively and applied successfully for the degradation of organic pollutants in aqueous solutions.

GRANT SUPPORT DETAILS

The authors would like to thank the Research Council in the Sultanate of Oman for funding (BFP/GRG/EBR/19/005) the research project. Authors are also grateful to the Natural and Medicinal Sciences Research Center at the University of Nizwa, Oman for providing the facilities and support to accomplish this research.

CONFLICT OF INTEREST

The authors declare that there are no conflicts of interest. Compliance with Ethical Standards : This article does not contain any studies involving human or animal subjects.

LIFE SCIENCE REPORTING

No life science threats were practiced in this research

REFERENCES

Alayan, H., et al. (2018). Hybrid carbon nanomaterial via CVD for methylene blue removal. Water Sci. Technol., 77, 1714–1723. https://doi.org/10.2166/wst.2018.057

Alayan, H.M., et al. (2019). Growth and optimization of CNTs in powdered activated carbon. Environ. Technol., 40, 2400–2415. https://doi.org/10.1080/09593330.2018.1441911

Alhussain, H., et al. (2024). Photocatalytic degradation of methyl orange using CuO/Al2O3 nanocomposite. Inorg. Chem. Commun., 162, 112272. https://doi.org/10.1016/j.inoche.2024.112272

Aljumaily, M., et al. (2018). Optimization of synthesis of superhydrophobic carbon nanomaterials by CVD. Sci. Rep., 8, 2778. https://doi.org/10.1038/s41598-018-21051-3

Al-Qaradawi, S., & Salman, R. (2002). Photocatalytic degradation of methyl orange as a model compound. J. Photochem. Photobiol. A, 148, 161–168. https://doi.org/10.1016/S1010-6030(02)00086-2

Al-Saadi, M., Muyibi, S., Alam, M., Ahmed, Y.M., & Sopyan, I. (2011). Synthesis of various carbon nanomaterials on powdered activated carbon. Afr. J. Biotechnol., 10, 18892–18905. https://doi.org/10.5897/AJB11.2771

Aroob, S., et al. (2023). Green synthesis and photocatalytic activity of CuO nanoparticles. Catalysts, 13, 502. https://doi.org/10.3390/catal13030502

Avasarala, B.K., Tirukkovalluri, S.R., & Bojja, S. (2010). Alkaline earth metal doped titania photocatalysts. Indian J. Chem. A, 49, 1189–1196.

Baqer, A., et al. (2018). Copper oxide nanoparticles synthesized by heat treatment: structural, morphological and optical characteristics. J. Mater. Sci. Mater. Electron., 29, 1025–1033. https://doi.org/10.1007/s10854-017-8002-3

Dana, A., & Sheibani, S. (2021). CNT–CuO nanocomposite photocatalyst with high visible-light efficiency. Adv. Powder Technol., 32, 3760–3769. https://doi.org/10.1016/j.apt.2021.08.023

Datsyuk, V., et al. (2008). Chemical oxidation of multiwalled carbon nanotubes. Carbon, 46, 833–840. https://doi.org/10.1016/j.carbon.2008.02.012

Demarema, S., et al. (2024). Green synthesis of metal oxide photocatalysts: bibliometric and techno-economic evaluation. J. Clean. Prod., 463, 142679. https://doi.org/10.1016/j.jclepro.2024.142679

Domagała, K., et al. (2020). Synthesis of copper-based multi-walled carbon nanotube composites. Arch. Metall. Mater., 65, 157–162. https://doi.org/10.24425/amm.2019.131109

Feng, Y., et al. (2019). Carbon nanotube–Cu2O nanocomposites as catalysts for p-nitrophenol reduction. Nanoscale Res. Lett., 14, 1–9. https://doi.org/10.1186/s11671-019-2914-1

Hameed, B.H., & Lee, T.W. (2009). Degradation of malachite green by Fenton process. J. Hazard. Mater., 164, 468–472. https://doi.org/10.1016/j.jhazmat.2008.08.018

Khan, S., et al. (2024). Photocatalytic dye degradation from textile wastewater: a review. ACS Omega, 9, 21751–21767. https://doi.org/10.1021/acsomega.4c00887

Kumar, A. (2017). Photodegradation of methyl orange by visible-light-active Co:La:TiO2 nanocomposite. J. Chem. Sci., 129, 164–174.
Kumar, A., & Pandey, G. (2017). Photocatalytic degradation of methyl green using Ni:La:TiO2 nanocomposites. IOSR J. Appl. Chem., 10, 31–44. https://doi.org/10.9790/5736-1009013144
Kumar, K.H., et al. (2025). Review on nano metal oxides for photocatalytic dye degradation. Sustain. Chem. One World, 6, 100055. https://doi.org/10.1016/j.scowo.2025.100055
Lau, G.E., et al. (2020). Eco-friendly photocatalysts for degradation of dyes. Catalysts, 10, 1129. https://doi.org/10.3390/catal10101129
Ma, Y., et al. (2018). Optimization of malachite green removal by TiO2 nanoparticles. Nanomaterials, 8, 428. https://doi.org/10.3390/nano8060428
Mahmoodi, N.M., et al. (2016). CuO/CNT nanocomposite for photocatalytic dye degradation. Fibers Polym., 17, 1842–1848. https://doi.org/10.1007/s12221-016-6645-y
Manasrah, A.D., et al. (2018). Surface modification of CNTs with CuO for nanofluid heat transfer. RSC Adv., 8, 1791–1802. https://doi.org/10.1039/C7RA10406E
Marques Neto, J., et al. (2017). Enhanced photocatalytic activity of iron oxide/CNT nanocomposites. J. Braz. Chem. Soc., 28, 2301–2312. https://doi.org/10.21577/0103-5053.20170081
Mohammed, S., et al. (2018). NiO–V2O5 nanocomposite for methyl orange degradation. Heliyon, 4, e00581. https://doi.org/10.1016/j.heliyon.2018.e00581
Moumen, A., et al. (2022). P-type metal oxide semiconductor thin films. Sensors, 22, 1359. https://doi.org/10.3390/s22041359
Nesaraj, A.S. (2014). Co3O4 nanoparticles for photocatalytic applications. Iran. J. Catal., 4, 219–226.
Nguyen, C.H., et al. (2019). Enhanced dye removal by photocatalysis over TiO2/ZnO/rGO composites. Sep. Purif. Technol., 232, 115962. https://doi.org/10.1016/j.seppur.2019.115962
Ping, C., & An-juan, W. (2016). CNTs/CuO synthesis and catalytic performance. J. Saudi Chem. Soc., 20, 343–348. https://doi.org/10.1016/j.jscs.2014.09.010
Rahmati, R., et al. (2021). Effect of hydrogen peroxide in photocatalytic dye removal. Water Sci. Technol., 83, 2414–2423. https://doi.org/10.2166/wst.2021.136
Rashed, M.N., & El-Amin, A. (2007). Photocatalytic degradation of methyl orange under solar irradiation. Int. J. Phys. Sci., 2, 73–81.
Reza, K.M., et al. (2017). Parameters affecting photocatalytic dye degradation using TiO2. Appl. Water Sci., 7, 1569–1578. https://doi.org/10.1007/s13201-015-0367-y
Rochkind, M., et al. (2014). Using dyes for evaluating photocatalytic properties. Molecules, 20, 88–110. https://doi.org/10.3390/molecules20010088
Salama, A., et al. (2018). Photocatalytic degradation using composite nanofibers. Appl. Nanosci., 8, 155–161. https://doi.org/10.1007/s13204-018-0660-9
Sapkota, K., et al. (2020). Visible-light photocatalysis of CuO/SWCNT nanocomposites. Catalysts, 10, 297. https://doi.org/10.3390/catal10030297
Shaban, M., & Ashraf, A.M. (2018). TiO2 nanoribbons/CNT composite. Sci. Rep., 8, 1–17. https://doi.org/10.1038/s41598-018-19172-w
Sharifpour, E., et al. (2022). CNT–ZnS/CuO nanocomposites for dye removal. Sci. Rep., 12, 12381. https://doi.org/10.1038/s41598-022-16676-4
Singh, S., et al. (2025). Photocatalytic degradation mechanisms of pollutants. Catal. Rev., 67, 1–49. https://doi.org/10.1080/01614940.2024.2440664
Wu, H.Q., et al. (2002). Synthesis of copper oxide nanoparticles using CNT templates. Chem. Phys. Lett., 364, 152–156. https://doi.org/10.1016/S0009-2614(02)01301-5
Youssef, N.A., et al. (2016). Degradation of methyl orange using Fenton reaction. Egypt. J. Pet., 25, 317–321. https://doi.org/10.1016/j.ejpe.2015.07.017